[1]Kumar R.

[2]Dr. S. Pazhanirajan

Oropharyngeal Cancer Diagnosis Using Deep Learning Technique with CNN

Abstract: - A cancer with a high severity that is widespread and complex is oral cancer. With 130,000 fatalities each year, oral cancer ranks as the eighth most frequent cancer worldwide in India. Salivary glands, tonsils,mouth and the neck are among areas where the tumour can be found. For example, a biopsy involves taking a small tissue sample from a body component and examining it under a microscope. There are also other screening techniques. However, the drawback is that it is impossible to distinguish between cancer cells and normal cells, and it is also impossible to categorise how many cells are impacted. In this study, cancer cells will be found and categorised in the oral region using digital processing technology. The most effective deep learning method was tested against a histopathological and real-time dataset. VGG16,ResNet50,MobileNetV2, DenseNet, and VGG19 were the 5 deep learning models utilised in this study. Classification Accuracy, Recall Rate,Error Rate, and Precision Rate are used to compare the effectiveness of the suggested approach. The results of the evaluation showed that ABC, FPSO, and CNN work better together to identify oral cancer.

Keywords: python, oral cancer, convolutional neural network, screening, optimization algorithm

1. INTRODUCTION

One of the most prevalent cancers in the world, oral cancer is distinguished by late diagnosis, high fatality rates, and morbidity. In 2018, GLOBOCAN predicted 177,384 fatalities and 354,864 new cases. In low- and middle-income nations (LMICs), oral cancer incidence accounts for two-thirds of all occurrences worldwide, with half of those instances occurring in South Asia. The two main risk factors for oral cancer are excessive alcohol use and tobacco use in any form. According to earlier research conducted in India, screening has led to early detection, disease downstaging, and a decrease in mortality among cigarette and alcohol users. Due to the lack of specialists and healthcare resources, LMICs bear a disproportionately large share of the burden of oral cancer, making it imperative that screening programmes provide an affordable and effective method of detection. The usage of telemedicine would be such an effective strategy . It revealed a moderate to high degree of agreement between the clinical conclusions reached by experts conducting a COE and those reached after they examine photographs taken with mobile devices.

Oropharyngeal cancer is a significant health concern globally, particularly in regions like India, where its prevalence contributes to substantial mortality rates. The complexity and widespread nature of this cancer pose challenges for accurate and efficient diagnosis. Traditional methods, such as biopsy and screening techniques, have limitations in distinguishing cancerous cells and assessing the extent of cellular impact. In response to these challenges, this study employs digital processing technology and evaluates various deep learning models, including VGG16, ResNet50, MobileNetV2, DenseNet, and VGG19, to enhance the diagnosis of oropharyngeal cancer. The research aims to improve the accuracy and effectiveness of identifying cancer cells within the oropharyngeal region, offering a potential breakthrough in diagnostic capabilities for this critical health issue.

Heoet al (2022)defines that according to several studies, tongue cancer is the most prevalent form of oral cancer (65%). Oral cancer is one of Asia's sixth most common malignancies and is more common in people from Asia (65.8%). Asians have a higher risk of oral cancer due to their lifestyle choices, which include things like chain smoking, heavy alcohol use, and betel nut consumption. **Wang & Fei (2022)** The physical border of tongue cancer, the most prevalent OC, is well defined. The peritumoral tissues, an essential part of the microenvironment, are involved in metastasis and recurrence and carry information related to tumour aggressiveness.

[1] Research Scholar, Department of Computer Science and Engineering, Faculty of Engineering and Technology, Annamalai University, Chidambaram. Assistant Professor, MVJ College of Engineering, Bangalore. Email: rkumarmecse@gmail.com

[2]Assistant Professor, Department of Computer Science and Engineering, Faculty of Engineering and Technology, Annamalai University, Chidambaram.

Shan et al (2020) demonstrates thatthe help of a finite number of discrete temperature measurements, a computer approach had been developed to estimate the parameters of the tumour. **Arathy (2022)** The parameters were optimised using the Levenberg-Marquardt (LM) technique after a Pennes bio heat transfer equation model of heat transmission in a closed mouth.

Phanthunane et al (2022)elaborately describes that the incidence of oral cancer, a malignant tumour that develops in the mouth cavity, ranges from 1% to 5% of all malignant tumours; however, the number of oral cancer cases has risen recently. **Kawamura & Kohei1 (2022)**Approximately 40% of instances of oral cancer are squamous cell carcinomas, which mostly involve the tongue. 1 Even though oral cancer can be seen by patients, many patients see specialised medical facilities at a very advanced stage defined in.

Kim et al (2021) Stage of the tumour at the time of diagnosis and therapy have been linked to survival among people with oral cancer. They also came to the conclusion that age and sex had no bearing on survival and thatpatients who had had radiotherapy alone had a worse survival rate than those who had received both radiotherapy and surgery.**Jubair et al (2022)** discovered, however, that a lower age was linked to a higher 5-year relative survival rate. A basic transfer learning model that makes use of a little deep CNN and a pretrained EfficientNet-B0 was proposed. A set of 716 clinical images served as training and testing grounds for the proposed model.

Zhu & Xiaolong (2023)illustrates that the dataset including participants with and without stomach cancer was developed after a total of 703 tongue images were collected using a custom tongue image capture tool. The Deeplabv3+ network was used to segment the tongue to lessen interference with feature extraction because the pictures captured by this equipment include non-tongue regions.

Chaudharyet al (2017) However, a significant portion of individuals who undergo a pathological examination do not have metastases (pN0). [13] When making clinical decisions and determining the prognosis for squamous cell carcinoma (SCC) of the oral tongue and mouth floor, histologic grade assessment is crucial (FOM).

Shi & Yu-lin (2022) The modernisation of TCM has ushered in new opportunities and problems as a result of recent advancements in TCM diagnostic information technology. There are a number of tongue diagnostic techniques that are often used in clinical settings, and technology for collecting and analysing objective data has been constantly improving based on standardised tongue diagnosis.

Dharani et al (2021) Salivary glands, tonsils, the neck, face, and mouth are among areas where the tumour can be found. A biopsy, for instance, entails extracting a little piece of tissue from an organ or other bodily part and studying it under a microscope. There are also other screening techniques. However, the drawback is that it is impossible to distinguish between cancer cells and normal cells, and it is also impossible to categorise how many cells are impacted.

Bansal (2022) For oral cancer, there are many different diagnostic methods, however they are only capable of precisely identifying cancer cells. Deep transfer learning methods were used to interpret images of oral cancer, both benign and malignant, using histopathologic and real-time datasets. These methods included ResNet50, MobileNetV2, VGG19, VGG16, and DenseNet.

1.1 Motivation of the paper

The motivation behind this study stems from the alarming prevalence and severity of oral cancer, particularly in India, where it ranks as the eighth most common cancer with 130,000 annual fatalities. Conventional diagnostic methods like biopsy and screening techniques have limitations in distinguishing between cancerous and normal cells, as well as assessing the extent of cell impact. To address these challenges, the study leverages digital processing technology and deep learning models, including VGG16, ResNet50, MobileNetV2, DenseNet, and VGG19, to detect and categorize oral cancer cells. The aim is to improve accuracy and efficiency in the identification of cancer cells within the oral region.

2. Methodology

Figure 1 depicts the overall organisation of this project. On top of the figure lies the training procedure. The example data includes both the training oral cancer photographs and the relevant cancer sorts. Separate the oral

cancer components after that. The trained classifier model is saved for future use after being trained using the retrieved attributes. The testing technique is shown at the bottom of Figure 1. Before the online processing begins, the sample is pre-processed using techniques like ABF to reduce noise and HE to increase clarity. Following pre-processing, the ABC approach is used for segmentation. Combining the two approaches yields features like texture and intensity, which are used to determine the distinctive traits. To shorten the execution time, a suitable feature is chosen after retrieving the features. Finally, based on the chosen features, the disease and its effects are found. Zernike moments, oriented gradient histograms, and wavelet-based features are the three feature extraction methods employed in this work.

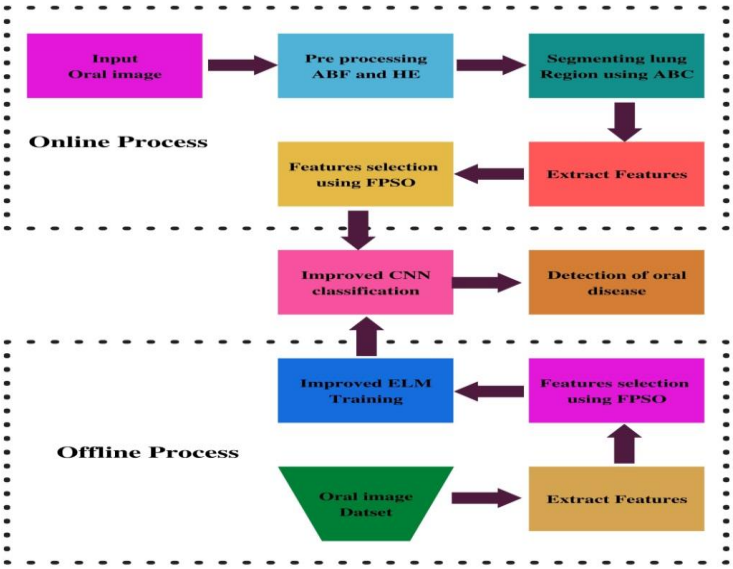

Figure 1. Working Procedure for the Proposed Work

2.1 Pre-processing

The histogram (HE) alignment approach was used to adjust the brightness of the incoming CT scan before continuing. Equation shows how His Excellency changed the brightness of the image to increase contrast (1). Let I x from the I y matrix be represented by the scanned image, with pixel intensities ranging from 0 to 256. Figure 1's normal histogram for intensity is indicated by the letter N.

$$I_N = \frac{\text{Number of pixels with available intensity}}{\text{Total number of pixets}} \quad (1)$$

Where n = 0,1,.....,256.

The enhanced image can be seen in Figures 2.

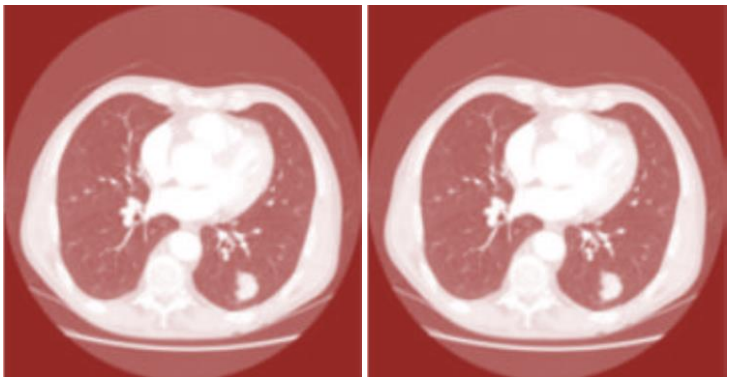

Figure. 2. created from a histogram (a) Introducing Oral Picture 2 (b) an equalisation histogram result

The Adaptive Bilateral Filter (ABF), which is indicated in Eq., is then used (2). To add more noise to the oral image in this piece, ABF is utilised.

$$\sum_{N=N_0-N}^{N0+N} \sum_{Y=Y_0-N}^{Y_0+N} \exp\left(-\frac{(X-X_0)^2+(Y-Y_0)^2}{2\nabla_d^2}\right) \text{X} \exp\left(-\frac{\text{G[m,n]}-\text{G}(X_0Y_0)^{\square}-(X_0Y_0)^2}{2\nabla_r^2[X_0Y_0]}\right) \text{-------} (2)$$

ABF uses a low-frequency, constant-frequency filter. Additionally, by enhancing the edge gradient, the ABF sharpens the image. Equation is used in ABF to calculate (3).

$$\delta[x_0, y_0] = \begin{cases} \text{MAXIMUM}\left(\beta_{x_0,y_0}\right) - G[x_0, y_0], \text{ if } \Omega_{x_0,y_0} > 0 \\ \text{MINIMUM}\left(\beta_{x_0,y_0}\right) - G[x_0, y_0], \text{ if } \Omega_{x_0,y_0} < 0 \\ 0, \quad \text{if } \Omega_{x_0,y_0} = 0 \end{cases} \text{----------} (3)$$

The centre point [x_ (0,) y 0] is used to represent every pixel. Let MAXIMUM and MINIMUM stand in for each action for retrieving a data value. effectiveness of fixed douchean filters and efficient range filters. In this case, (d) = 1 is a constant, and (r) modifies the value as shown in the Figure. (3).

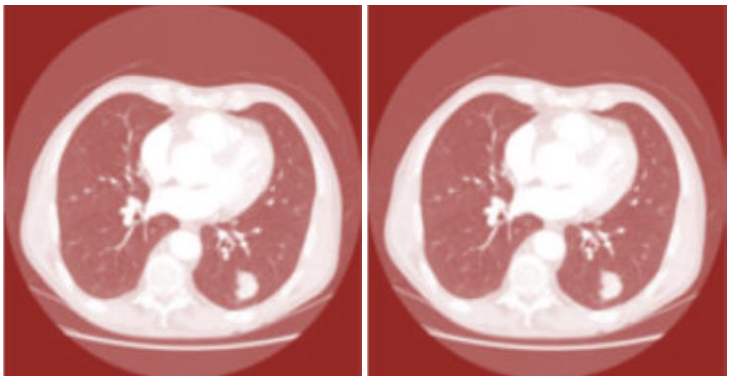

Figure 3. (a) The outcome of histogram equivalence (b)Noisy Image Removed

2.2 Deep Learning Model: -

For classification, various Deep Learning models like MobileNetV2, VGG16, DenseNet,VGG 19, and ResNet50 were utilised..

VGG16 and VGG19:- The Visual Geometry Group is known as VGG. The 33 kernel-sized filters that make up VGG16 are employed in a sequential manner . A RGB image measuring 224x244 is the VGG input. The network, which has 19 layers, can recognise images in a range of categories. The basic goal of the VGG designs is to build an extremely deep network while maintaining a minimal and constant convolution size.

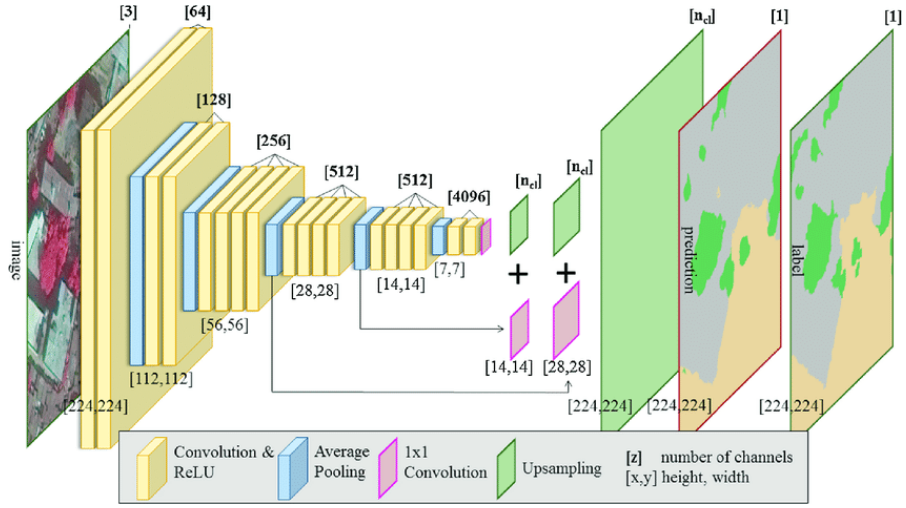

Figure 4: VGG-19 architecture

MobileNetV2:-A novel module with an inverted residual structure is presented in MobileNetV2. Modern semantic segmentation and object recognition are made possible by MobileNetV2. The first design layer of MobileNetV2 is a fully convolutional layer that has 32 filters and 19 bottleneck layers. 3.4 million parameters and 300 million multiply-add operations are frequently used by the network. Accuracy is increased by removing ReLU6 from each bottleneck module's output.

DenseNets:-The moniker "densely linked convolutional network" refers to the close connections between each layer in a DenseNet design. Direct connections between "L" levels are L(L + 1)/2. The feature maps from prior levels are pooled and used as inputs in each layer rather than being averaged.

2.3Segmentation

Pre-processed images are divided into regions by the segment, which looks for objects or boundaries that assist extract the necessary bits of the image. The procedures stated above were originally classified using the ABC division approach, as shown in Figure 4. Classification requires removing the damaged cells from a CT scan taken before surgery. To divide the oral cancer, techniques including K-Means, FCM, and Ant Colonywere used. Longer computation time is required by the FCM algorithm. It responds to local noise and slow speeds.

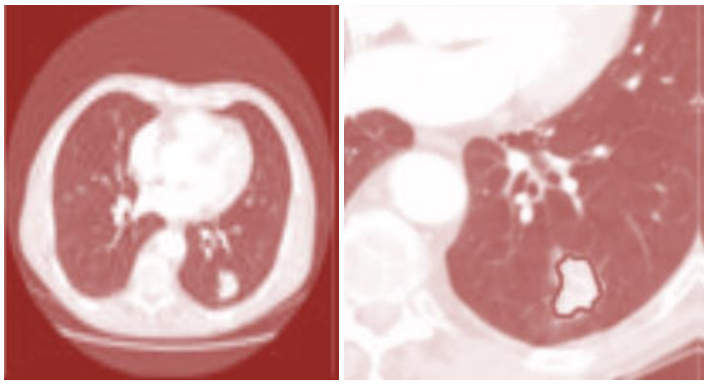

Fig.5 (a)Noise-Reduced Image (b)ABC Result

2.4 Feature Extraction

The segmentation produces two features: texture and intensity. To extract texture, LBP and wavelet methods are used. 140 features are excerpted in this study, including 97 Zernike moments, 27 wavelet features, and 19 CVH features.

2.5 Wavelet attributes

Wavelets play a significant and common role in describing properties in texture retrieval. The multi-resolution properties and fundamental frequency data are well captured by wavelet technology. This is the point when the H-level breaks down, creating different 3H + 1 bands. The HL picture decomposition was built using the LH frequency subgroup, which also supplied the HH horizontal image data required to produce the image's diagonal characteristics.

2.6CVH attributes

CVH stands for the CT value histogram. Each return on investment is represented by a CT value histogram. Experimental analysis was used to calculate the histogram's container count.

2.7 Zernike moment features

The transformation and extension of the tables in the ROI determine Zernike's time. In particular, the Zernike moments on two similar pictures that are neither extended or otherwise interpreted differ. Zernike dependence issues are resolved using two different approaches. Every picture mass's centroid is converted to the ROI's corresponding ROI's centre. This process eliminates Zernike time's reliance on object modification.

2.8 Feature Selection

In order to produce high-quality categorization results, multiple types of features are used simultaneously. By choosing discriminant features from a variety of feature spaces, classification effectiveness may be improved since various types of characteristics could have additional information. The purpose of the distinctive feature set can be defined thanks to feature assortment. For selecting features, fuzzy particle swap optimization (FPSO) is used.

2.9 Fuzzy Particle Swam Optimization (FPSO)

Along with the information foundation, it makes sense. PSO stands out among other algorithms like DE, PSO, and GA because it offers standout qualities including lower costs and solutions that are guaranteed to be optimal. Through the use of a fuzzy variable, the particle's influence on others nearby is overpowered.

2.10 Classification

2.10.1 ELM Classifier

Use the ELM forward neural network for functional training and single-layer or multi-layer hidden node classification without having to establish hidden node limits. The ELM classification tool's weight between the hidden and output layers is W2, as seen in the graphic below. gives the outcome and the hidden layer the same amount of weight. The realisation function (x) may be calculated by multiplying this by q. There is little room for improvement in ELM as seen in Figure 5. The ELM approximation theorem allows for the use of unrelated functions as output functions, provided that they are connected to the sequence in hidden layers. The core matrix may be seen in the image below (K).

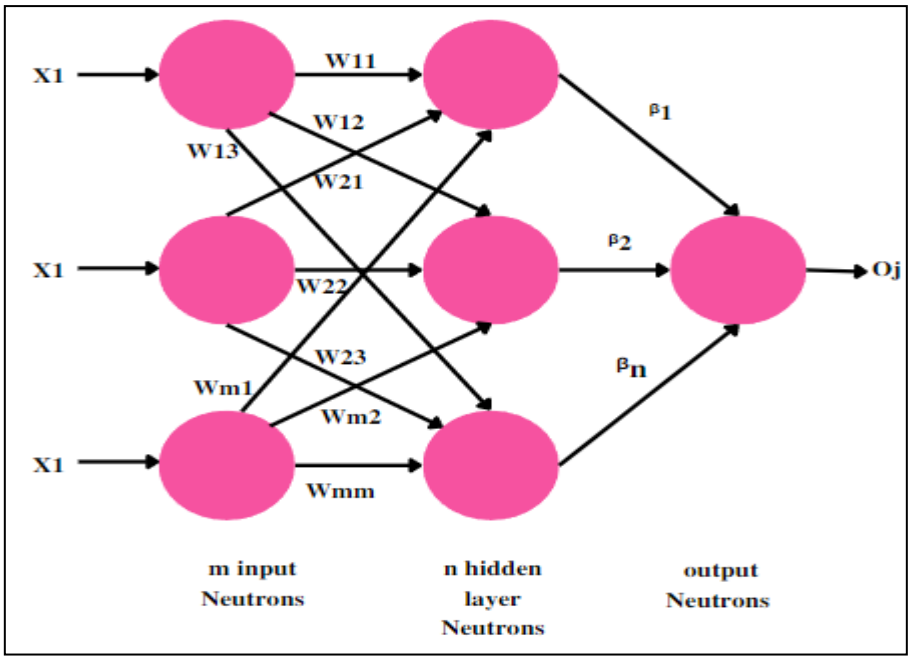

Figure 6. ELM Architecture

$q = W2\sigma(W1X)$ ---------- (4)

Where k (x m, x n) is the function of the nucleus of the hidden neuron and Q is the resulting matrix of the hidden layer. Equation defines the ELM outcome (5).

$K = k(Xm, Xn) = q(Xm)q(Xn) = QQT$ ---------- (5)

2.10.2CNN Classifier

In a normal neuron, the input is received, the point product is computed, and the behaviour is non-linear. In addition to convolutional layers, each Convolutional Neuron Network also has pooling layers and subsampling levels. It is common practice to use convolutional neural networks for the purpose of cancer cell type and

severity classification. It is possible to do down sampling using the CNN's pooling layer. Reducing the quantity of features extracted in convolution layers decreases time consumption, as seen in Figure.6.

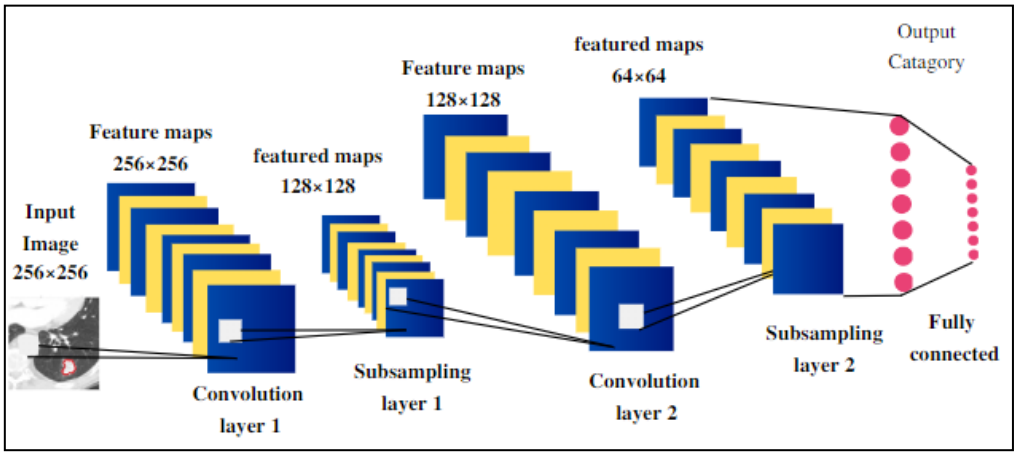

Figure 7. CNN-Based Oral Cancer Diagnosis

With this layer's answer as input, the convolutional neural network moves on to the next layer. Below is the algorithm that reveals the method for CNN-based classification.

1. Convolution filter first layer application

2. Convolutional filters are less sensitive once they have been smoothed.

3. The process layer checks each layer that the signal passes through.

4. Limit training sessions using the Rectified Linear Unit (RELU)

5. The neurons in the flow layer are linked to all the neurons in the layer below.

6. To suggest neural networks during offline processing, add a layer of loss at the conclusion.

2.11 CNN Python analysis:

def prepare_and_load(isval-True):

Arrange

if isval==True:

normal_dir=val_dir/"NORMAL"

pneumonia dir-val_dir/'PNEUMONIA

else:

normal dir-test_dir/'NORMAL'

pneumonia dir-test_dir/'PNEUMONIA normal_cases-normal_dir.glob(".jpeg") pneumonia_cases = pneumonia_dir.glob(".jpeg") data, labels-([] for x in range(2))

def prepare(case):

for ing in case:

ing cv2.imread(str(img))

ing (224,224))

if img.shape[2] ==1:

img= np.dstack([ing, ing, img])

ing cv2.cvtColor(ing, cv2.COLOR_BGR2RGB)

inging.astype(np.float32)/255.

if case normal_cases:

label to categorical(e, num_classes-2) else:

label = to_categorical(1, num_classes=2)

data.append(img)

labels.append(label) return data, labels

prepare(normal_cases)

4,1-prepare(pneumonia_cases)

d-np.array(d)

1-np.array(1)

3. RESULTS & DISCUSSIONS

3.1 Data set

3.1.1 UCI Deep Learning Repository Data Set

To assess the effectiveness of CNN, UCI data collected from oral CT scans were taken into account and several classifications for mouth cancer. The lung nodes may be seen across most of this CT scan. Fig. 7 illustrates an illustration of an oral CT scan.

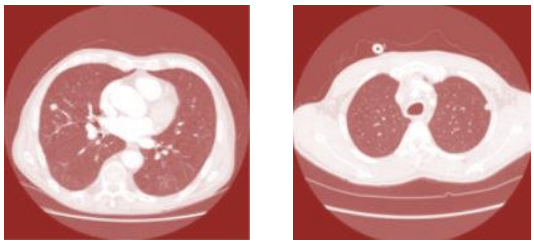

Figure8.ExamplesofUCIDeepLearningRepositoryDataSet

3.2 Utilised performance metrics

The division of malignant nodules that may be reliably predicted as shown in Equation is referred to as sensitivity (Sn) (6).

$$Sn = \frac{TrP}{TrP + FaN}$$

According to Equation, Specificity (Sp) is defined as the division of precisely predicted benign nodules (7),

$$S_p = \frac{T_rn}{T_rn+F_ap}$$

3.3 Classification Accuracy (CA)

$$CA = \frac{T_rP+T_rn}{T_rP+T_rn+F_ap+F_ap}$$

Where represents the number of accurately predicted malignant nodules in Equation (8).

3.4 Error Rate

The number of diseases that are incorrectly diagnosed in a particular image is measured by the error rate.

Error rate=Number of images categorized incorrectly

Total number of images.

3.5 Experimental Analysis

Trail no.1: Feature Derivative Methods Examination

This feature derivative scheme's performance is evaluated by comparing it to other methods utilising operating indicators including error rate, sensitivity, specificity, and accuracy. Table 1 lists the results of these indicators.

Table 1. Analyses of Feature Derivative Methods

UCI Deep learning repository data set				
Feature derivate				
Examination Parameter	ACC	SEN	SPEC	ERR
Wavelet	82.58	91.4	93.91	17.42
CVH	81.12	90.51	92.85	8.88
Zernike	82.71	89.82	93.8	17.29
All	91.651	92.451	92.321	8.349

The effects of the feature derivative techniques used in this test are effectively evaluated. The highest SEN is 98, as seen in Table 1. There is a value of 154 for the All feature, making it more potent than other methods because it is the greatest value.

Analysis of Partitioning Strategies for Oral Cancer

This feature derivative scheme's performance is evaluated by comparing it to other methods utilising operating indicators including error rate, sensitivity, specificity, and accuracy. Table 2 lists the results of these indicators.

Table 2.UCI Explores Oral Cancer Treatment Methods

UCI Deep learning repository data set				
Oral cancer partitioning				
Examination Parameter	ACC	SEN	SPEC	ERR
FCM	85.641	86.481	86.351	14.359
K-Means	84.161	85.021	84.891	15.839
ABC	94.161	94.971	94.841	5.839

The effects of the feature derivative techniques used in this test are effectively evaluated. Table 2 shows that, when compared to other strategies, ABC has the highest SEN (98.752), making it the most effective method.

Examination of Oral Cancer Classification Techniques

To compare our cancer classification system's performance to that of other approaches, we utilise sensitivity, error rate, accuracy, and specificity as operational indicators. Table 3 lists the results of these indicators.

Table 3. UCI Evaluation of Oral Cancer Classification Methods

UCI Deep learning repository data set				
Oral cancer Clasification				
Examination Parameter	ACC	SEN	SPEC	ERR
SVM	94.23	95.6	94.91	5.77
Bagging	89.26	90.75	89.95	10.74
Navie Bayes	85.71	86.63	86.42	14.29
KNN	84.23	85.21	84.96	15.77
Ada Boost	91.76	92.82	92.43	8.24
IELM	97.14	98.39	97.87	2.86
CNN	98.2	98.45	98.78	1.8

The results of the feature derivative methods used in this test are evaluated effectively. Table 3 shows that of the techniques tested, CNN has the best SEN (97.234), making it the most efficient.

As shown in fig. 8(a), training loss, accuracy, and precision after applying ResNet50 were shown to be easier to forecast on the training dataset than the validation dataset. It calculated 0.79 accuracy, 0.58 loss, 0.87 area under the curve, and 0.78 precision for the training phase. In a similar manner, it calculated 0.75 accuracy, 0.57 loss, 0.83 area under the curve, and 0.73 precision for the validation phase.

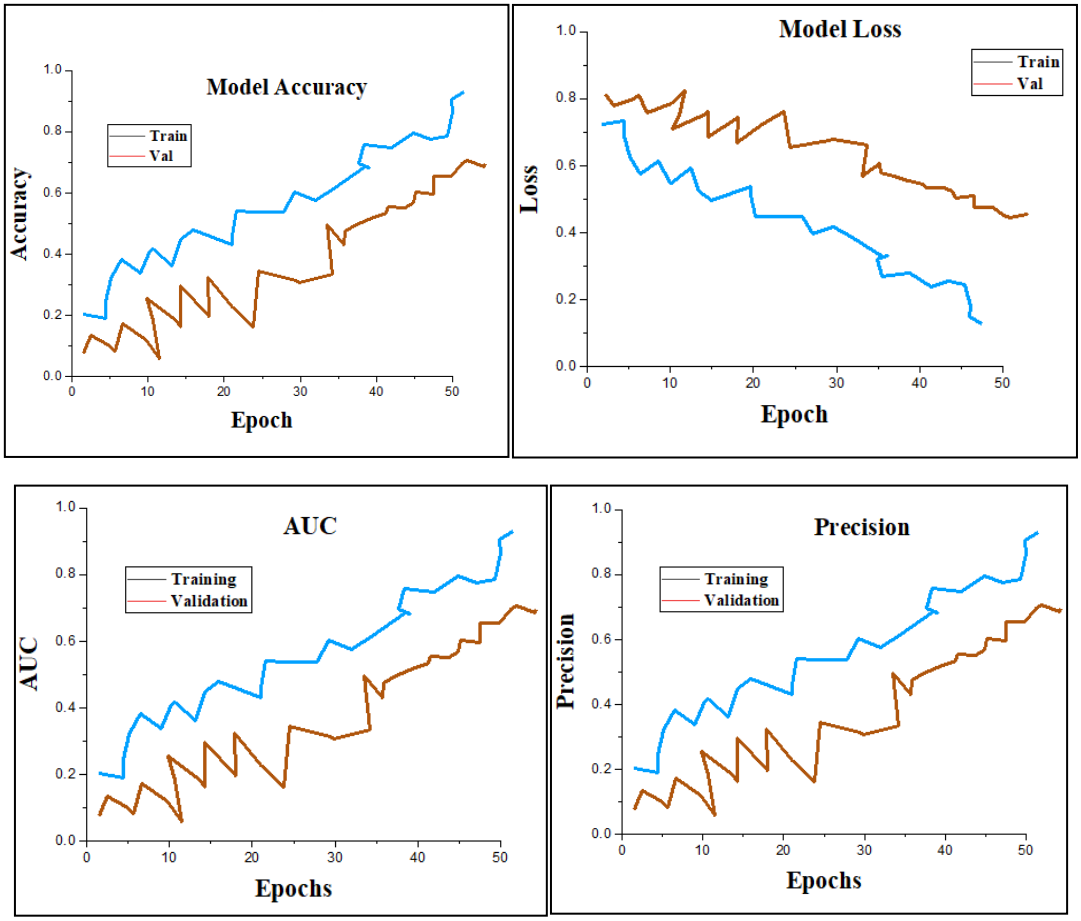

Figure 9(a) System performance of ResNet50

In a similar manner, it calculated 0.72 accuracy, 0.65 loss, 0.80 area under the curve, and 0.73 precision for the validation phase. As a result, the model is properly represented by the training dataset. As the plot of validation loss drops for VGG16, overfitting is a problem.

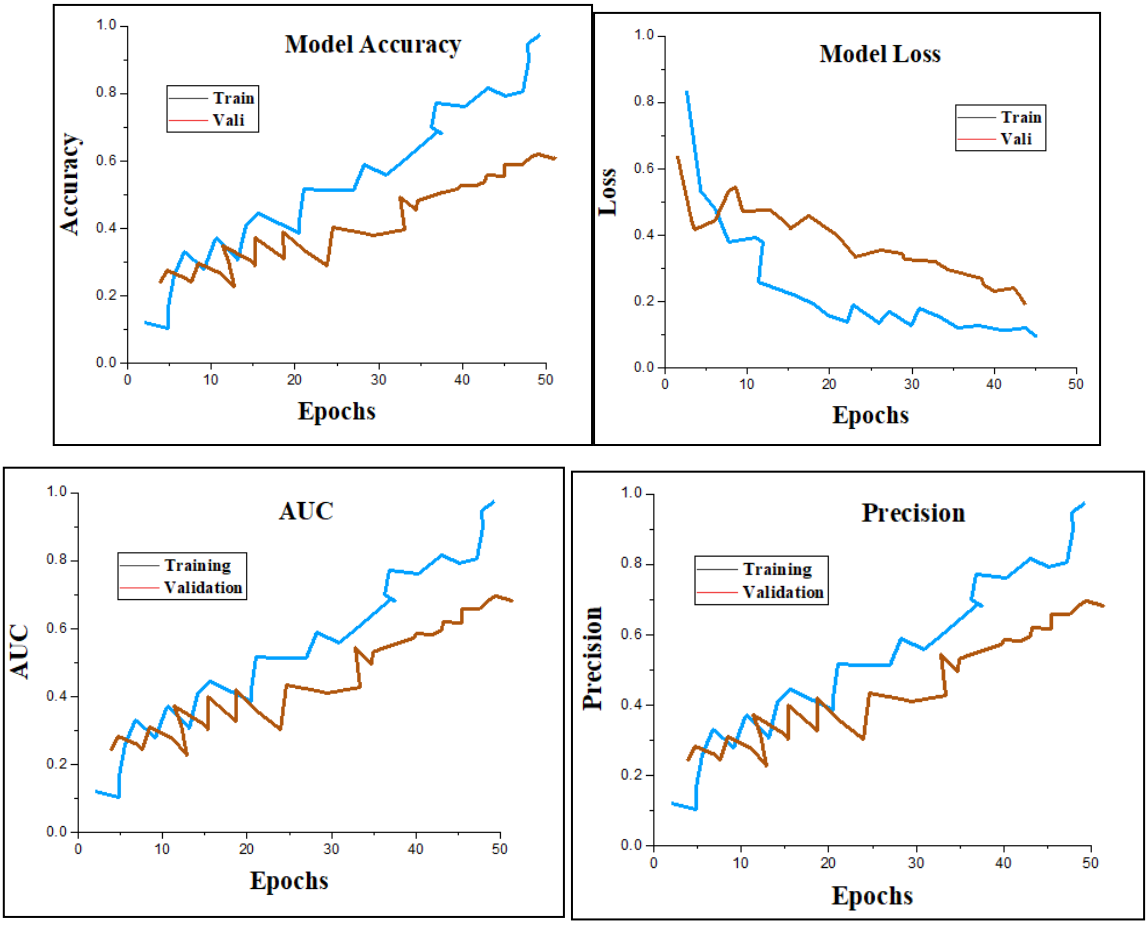

Figure 9 (b) System performance of VGG16

Figure 8(c) illustrates that the training dataset is easier to forecast than the validation dataset, as shown by greater training accuracy, loss, precision, and auc compared to validation accuracy, precision, and auc. It calculated 0.90 accuracy, 0.2 loss, 0.95 area under the curve, and 0.90 precision for the training phase. In a similar manner, it calculated 0.80 accuracy, 0.35 loss, 0.90 area under the curve, and 0.80 precision for the validation phase.

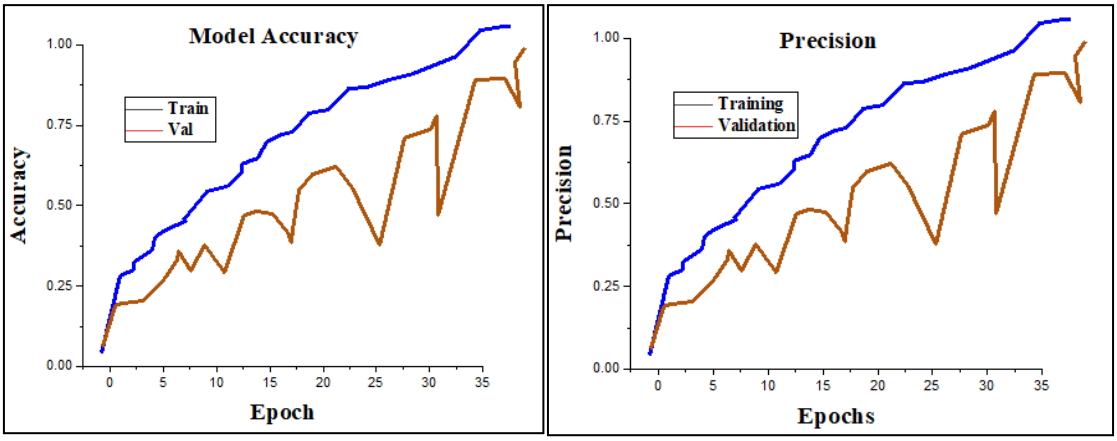

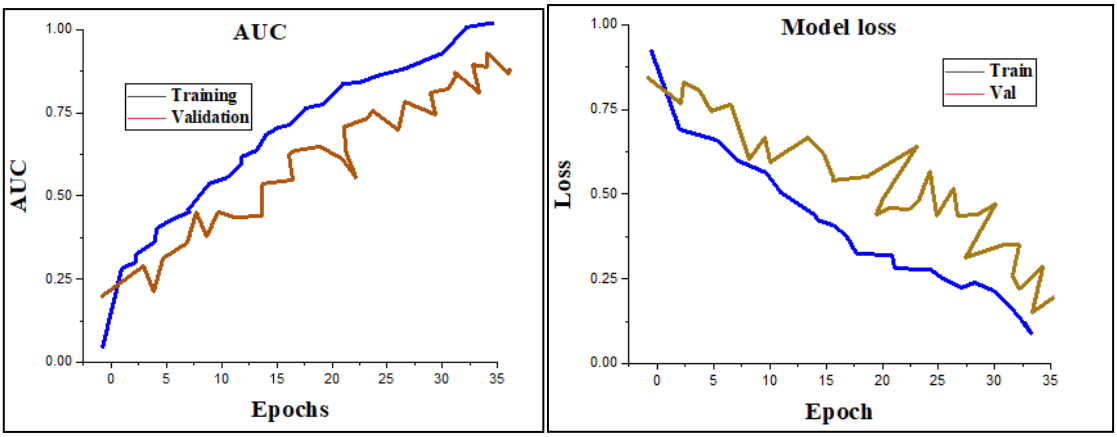

Figure 9(c) System performance of VGG19

Figure 8(d) shows that training loss, accuracy, and precision, auc are higher than validation precision, accuracy, and auc after the application of MobileNetV2. This suggests that the training dataset is simpler to predict than the validation dataset. It calculated 1.0 accuracy, 0.2 loss, 0.95 area under the curve, and 0.99 precision for the training phase. It calculated 0.80 accuracy, 0.6 loss, 0.90 area under the curve, and 0.80 precision during the validation phase.

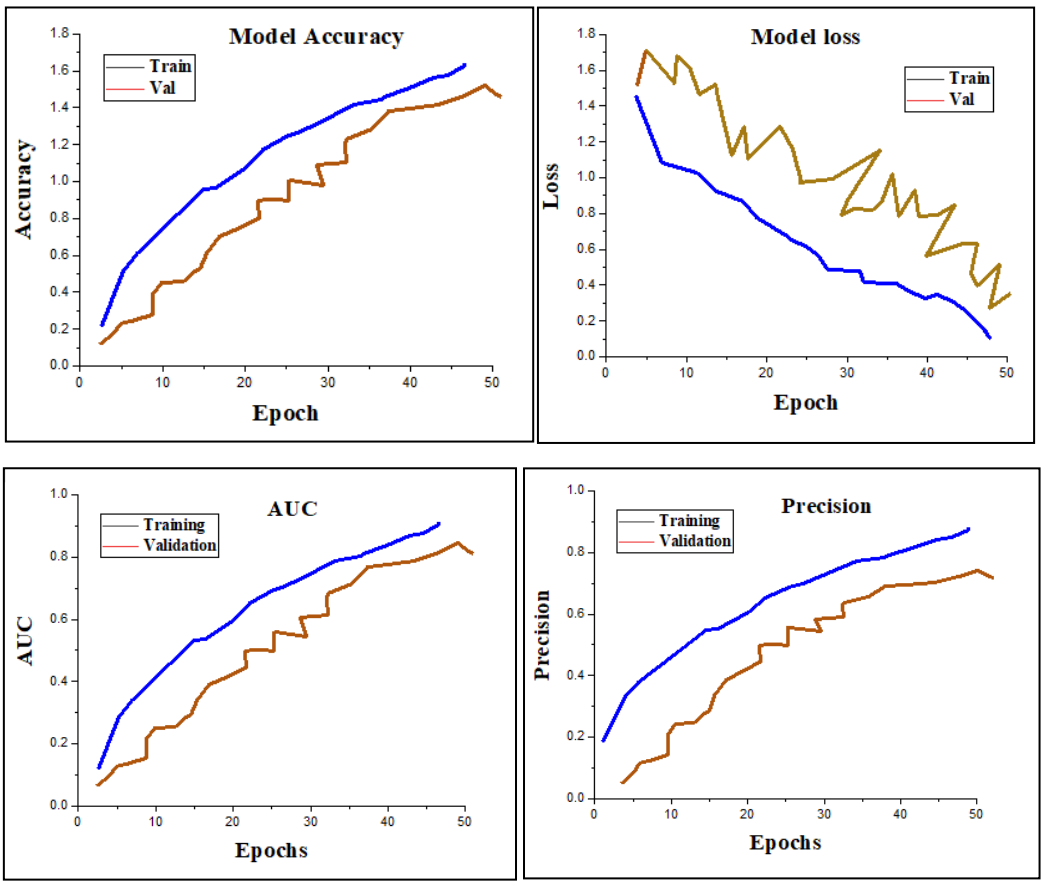

Figure 9 (d) System performance of MobileNetV2

While the validation dataset is more challenging to forecast, Figure 8(e) demonstrates that the training dataset surpasses the validation dataset in terms of loss, training accuracy, precision, and auc after using DenseNet. During training, it determined an accuracy of 0.1, a loss of 0.0, an area under the curve of 1.0, and a precision of 1.0. It calculated 0.9 accuracy, 0.4 loss, 0.95 area under the curve, and 0.90 precision for the validation phase.

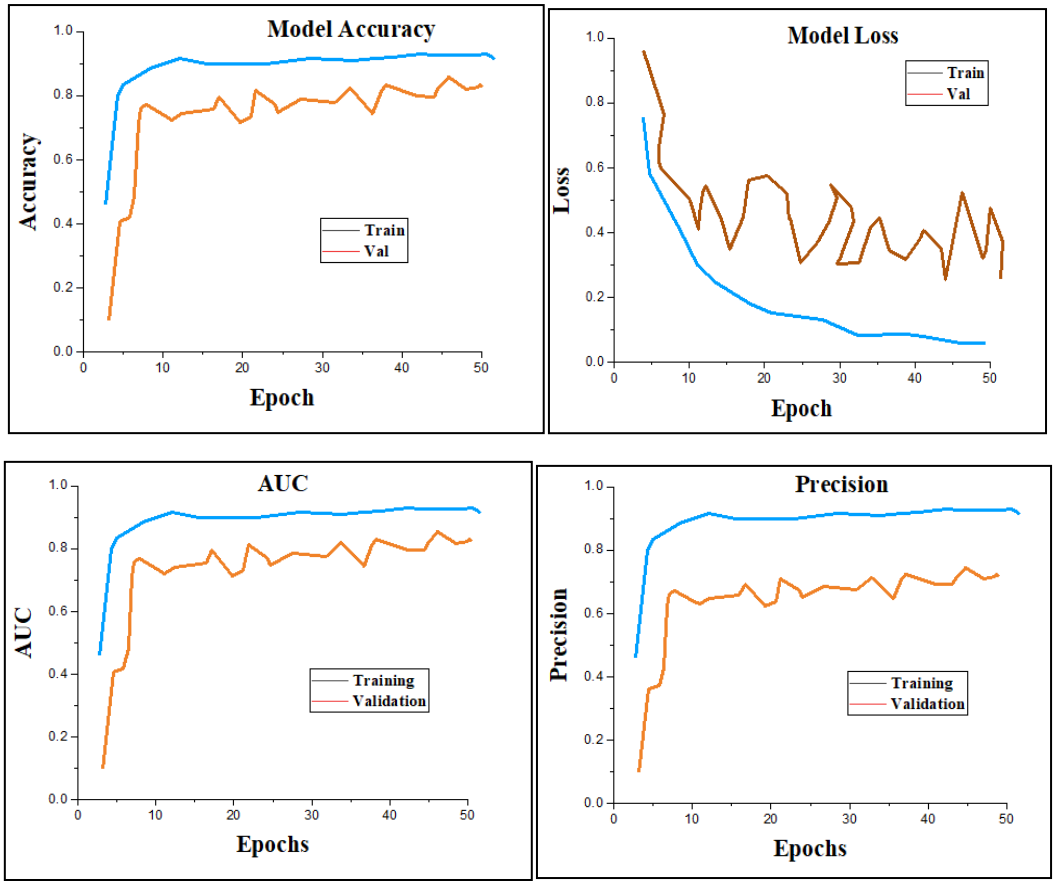

Figure 9 (e) System performance of DenseNet

4. Conclusion

A thorough comparison of approaches is carried out in this study that focuses on the detection of oral cancer using CT imaging. Findings show that CNN classifiers achieved an outstanding overall accuracy of 97.21%, demonstrating that this method is useful for detecting oral cancer in CT scans. The study uses important criteria including sensitivity, specificity, and error rate, and it shows that CNN is always better than other methods. The segmentation approaches are also thoroughly evaluated, and the results inform the combination of three methods—ABC, FPSO, and CNN—to create a novel automated system for oral cancer diagnosis in CT images. The work puts the suggested technique through its paces using a variety of deep learning models, including as VGG19, ResNet50, MobileNetV2, DenseNet, and histopathology and real-time datasets. By using cutting-edge deep learning techniques, this study makes a substantial contribution to improving automated oral cancer detection capabilities.

References

[1] Heo, Jaesung, et al. "Deep learning model for tongue cancer diagnosis using endoscopic images." *Scientific reports* 12.1 (2022): 6281.

[2] Wang, Fei, et al. "Magnetic resonance imaging-based radiomics features associated with depth of invasion predicted lymph node metastasis and prognosis in tongue cancer." *Journal of Magnetic Resonance Imaging* 56.1 (2022): 196-209.

[3] Shan, Jie, et al. "Machine learning predicts lymph node metastasis in early-stage oral tongue squamous cell carcinoma." *Journal of Oral and Maxillofacial Surgery* 78.12 (2020): 2208-2218.

[4] Arathy, K., et al. "Early Detection and Parameter Estimation of Tongue Tumour Using Contact Thermometry in a Closed Mouth." *International Journal of Thermophysics* 43 (2022): 1-16.

[5] Phanthunane, Chumut, et al. "Intratumoral niches of B cells and follicular helper T cells, and the absence of regulatory T cells, associate with longer survival in early-stage oral tongue cancer patients." *Cancers* 14.17 (2022): 4298.

[6] Kawamura, Kohei, et al. "Prediction of cervical lymph node metastasis from immunostained specimens of tongue cancer using a multilayer perceptron neural network." *Cancer Medicine* (2022).

[7] Kim, Yeongjoo, et al. "Novel deep learning-based survival prediction for oral cancer by analyzingtumor-infiltrating lymphocyte profiles through CIBERSORT." *Oncoimmunology* 10.1 (2021): 1904573.

[8] Jubair, Fahed, et al. "A novel lightweight deep convolutional neural network for early detection of oral cancer." *Oral Diseases* 28.4 (2022): 1123-1130.

[9] Zhu, Xiaolong, et al. "A Framework to Predict Gastric Cancer Based on Tongue Features and Deep Learning." *Micromachines* 14.1 (2023): 53.

[10] Chaudhary, Neena, et al. "Incidence of occult metastasis in clinically N0 oral tongue squamous cell carcinoma and its association with tumor staging, thickness, and differentiation." *Journal of Head & Neck Physicians And Surgeons* 5.2 (2017): 75.

[11] Shi, Yu-lin, et al. "Machine Learning Prediction Models for Different Stages of Non-small Cell Lung Cancer Based on Tongue and Tumor Marker." (2022).

[12] R. Dharani, S. Revathy et al "DEEPORCD: Detection of Oral Cancer using Deep Learning" Journal of Physics: Conference Series, Volume 1911, International Conference on Innovative Technology for Sustainable Development 2021 (ICITSD 2021) 27-29 January 2021,

[13] Bansal, K., Bathla, R.K. & Kumar, Y. Deep transfer learning techniques with hybrid optimization in early prediction and diagnosis of different types of oral cancer. *Soft Comput* 26, 11153–11184 (2022).